Size effect on the adsorption and dissociation of CO2 on Co nanoclusters

Yu, Haiyan; Cao, Dapeng; Fisher, Adrian; Johnston, Roy; Cheng, Daojian

DOI:
10.1016/j.apsusc.2016.10.192

Document Version
Peer reviewed version

Citation for published version (Harvard):
Yu, H, Cao, D, Fisher, A, Johnston, R & Cheng, D 2017, 'Size effect on the adsorption and dissociation of CO2 on Co nanoclusters', *Applied Surface Science*, vol. 396, pp. 539-546.
https://doi.org/10.1016/j.apsusc.2016.10.192

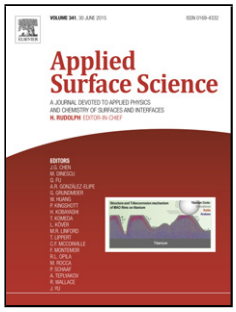

Title: Size Effect on the Adsorption and Dissociation of CO_2 on Co Nanoclusters

Author: Haiyan Yu Dapeng Cao Adrian Fisher Roy L. Johnston Daojian Cheng

PII: S0169-4332(16)32328-5
DOI: http://dx.doi.org/doi:10.1016/j.apsusc.2016.10.192
Reference: APSUSC 34286

To appear in: *APSUSC*

Received date: 30-7-2016
Revised date: 20-10-2016
Accepted date: 29-10-2016

Please cite this article as: Haiyan Yu, Dapeng Cao, Adrian Fisher, Roy L.Johnston, Daojian Cheng, Size Effect on the Adsorption and Dissociation of CO2 on Co Nanoclusters, Applied Surface Science http://dx.doi.org/10.1016/j.apsusc.2016.10.192

Size Effect on the Adsorption and Dissociation of CO_2 on Co Nanoclusters

Haiyan Yu[a], Dapeng Cao[a], Adrian Fisher[a], Roy L. Johnston[b], and Daojian Cheng[a*]

[a]*International Research Center for Soft Matter, State Key Laboratory of Organic-Inorganic Composites, Beijing University of Chemical Technology, Beijing 100029, People's Republic of China*

[b]*School of Chemistry, University of Birmingham, Edgbaston, Birmingham, B15 2TT, United Kingdom*

* Authors to whom correspondence should be addressed. Tel.: +86-10-64453523; fax: +86-10-64427616. Electronic addresses: chengdj@mail.buct.edu.cn (D. Cheng)

Graphical abstract

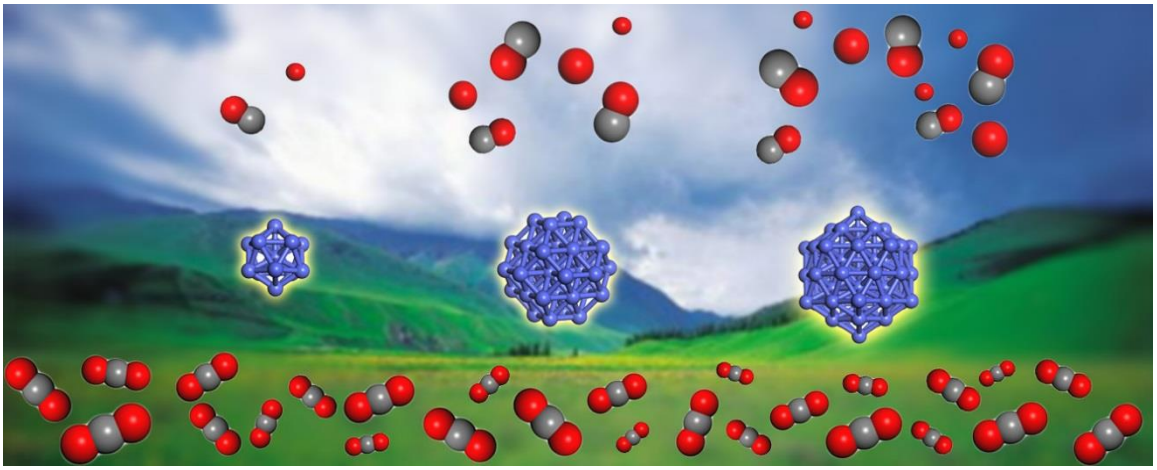

Research highlights

- Co_{13}, Co_{38} and Co_{55} nanoclusters were predicted as the high-symmetry structures.
- CO_2 dissociation on the size-selected Co_{13}, Co_{38} and Co_{55} nanoclusters was studied.
- Co_{55} nanocluster possesses the highest activity relevant to CO_2 dissociation.
- A non-monotonous behavior of the dissociation barrier of CO_2 with the size was found.

Abstract

Spin-polarized density functional theory calculations were carried out to study the adsorption and dissociation properties of CO_2 on size-selected Co_{13}, Co_{38} and Co_{55} nanoclusters. Based on genetic algorithm method, Co_{13}, Co_{38} and Co_{55} nanoclusters were predicted as the most stable high-symmetry structures among these Co_n (n = 2 to 58) nanoclusters from the Gupta potential. For the adsorption of CO_2, CO and O on size-selected Co_{13}, Co_{38} and Co_{55} nanoclusters, the lowest adsorption strength is found for all the different adsorbates on Co_{55} nanocluster. For the dissociation of CO_2 on these size-selected Co nanoclusters, the largest Co_{55} nanocluster possesses the greatest catalytic activity for the dissociation of CO_2, with the smallest reaction barrier of 0.38 eV. Our results reveal a non-monotonous behavior of the catalytic activities of Co nanoclusters on size, which is of fundamental interest for the design of new Co catalysts for the conversion of CO_2.

Keywords: Adsorption and dissociation of CO_2, Size effect, Co nanocluster, DFT calculations.

1 Introduction

In recent years, in addition to the capture and storage technology [1-7], the recycling technology for CO_2, a major greenhouse gas, has attracted considerable interest. A promising route for relieving the greenhouse effect is to convert CO_2 into CO, which has been widely investigated in the recycling technology. Subsequently, the converted CO could hydrogenate to organic chemicals such as methanol, or could be used directly in fuel cells or internal-combustion energies [8-12]. During the whole process, catalysts that promote the dissociation of CO_2 to CO play an important role in the recycling technology. Therefore, high efficient catalysts are urgent to be developed for the conversion of CO_2 into CO.

The catalytic activation of CO_2 by bulk transition metals (TM), especially Fe, Co, Ni, Cu, Au, Ru and Rh, has been broadly studied both experimentally and theoretically [13-21]. More recently, many studies have implied that nanoclusters possess excellent catalytic properties which are distinct from those of bulk metals possess. For instance, by providing a suitable adsorption region, a double icosahedral Ru_{19} nanocluster can significantly improve the CO_2 adsorption strength compared to the surface case, which further enhance the catalytic capability by lowering the energy barrier of CO_2 dissociation [20]. In addition, Chang and Ho [19] mentioned that the Rh(111) surface might be unable to adsorb a CO_2 molecule; however, free Rh_{13}-I_h nanocluster and unzipped graphene oxide–supported Rh_{13} nanocluster can adsorb CO_2 with the adsorption energies of -0.76 and -1.18 eV and break the corresponding C-O bond with the energy barriers of 0.83 and 0.45 eV. Moreover, Co has been experimentally confirmed to be a good catalyst for the conversion of CO_2 [22-24]. Iablokov *et al.* [22] found that the catalytic activity for the hydrogenation of CO_2 increases with the size of these Co nanoparticles from 3 to 10 nm. It confirmed the catalytic activity of Co nanoparticle catalysts for the hydrogenation of CO_2 is size-dependent. As mentioned above, Co nanoclusters could be promising for the dissociation of CO_2 to CO, and thus further studies are still necessary.

Recently, theoretical studies based on density functional theory (DFT) [25, 26] have been used to investigate the adsorption and dissociation mechanism of CO_2 on cobalt surfaces. For example, Fierro *et al.* [15] found the evidence for spontaneous activation of CO_2 on cobalt surfaces using DFT calculations. The molecule structure of CO_2 adsorbed on Co (100) and Co (110) surfaces is highly distorted, which means that the adsorbed CO_2 molecule can be activated spontaneously. Moreover, the size-dependent catalytic activities for the hydrogenation of CO_2 [22] and the dissociation of CO [27] on Co nanoparticles have been studied experimentally. Thus, a full understanding on the size-dependent adsorption and catalytic properties of

small Co nanoclusters by DFT calculations will be of fundamental interest for the design and application of these metal nanoclusters as catalysts [28]. However, to the best of our knowledge, there are still no theoretical studies focusing on the size-dependent adsorption and dissociation of CO_2 to CO on Co nanoclusters.

In this work, the adsorption and dissociation properties of CO_2 on size-selected Co_{13}, Co_{38} and Co_{55} nanoclusters were investigated by using spin-polarized density functional theory calculations. The Co_{13}, Co_{38} and Co_{55} nanoclusters were identified as the most stable structures with high symmetry in the range from Co_2 to Co_{58} based on the Gupta potential. The size-dependent adsorption of CO_2, CO and O and dissociation of CO_2 on Co_{13}, Co_{38} and Co_{55} nanoclusters were discussed. The density of states and charge density difference were calculated to understand the detailed adsorption and dissociation properties of CO_2 on these nanoclusters.

2 Calculation Details

Initially, the lowest-energy atomic ordering of Co_n (n = 2 to 58) nanoclusters was obtained by global optimization [29] at the Gupta empirical potential level, and then was subjected to DFT relaxation. The resulting configurations were used to study the adsorption and dissociation properties of CO_2.

Global optimization was performed using the Birmingham cluster genetic algorithm (BCGA) based on the Gupta potential [30, 31]. This method was well documented in the previous work [32-35] and was found to be effective to obtain the equilibrium structures of metal nanoclusters [36-39]. The genetic algorithm (GA) is a population-based search technique in global structural optimization [40]. It is based on principles of natural evolution, using operators which have analogues in the theory of biological evolution, such as mating, mutation, and natural selection. It explores many different solutions simultaneously and each investigation reveals information about a different region of the surface. BCGA acts on the phenotype (*i.e.*, the 3D cluster structure) rather than the genotype (encoded coordinates) [41, 42].

The interaction between metal Co atoms was semi-empirically modeled based on the well-established Gupta potential. It is noted that Gupta potential has been successfully used to model the structures of Co-based nanoclusters [43, 44]. The Gupta potential parameters for Co nanoclusters used in this study were taken from the literature [43], as listed in Table 1.

Spin-polarized DFT calculations were performed by using Quantum Espresso package [45], Plane-Wave Self-Consistent Field (PWscf). The Perdew-Burke-Ernzerhof (PBE) xc-functional [46] and ultrasoft pseudopotentials [47] were used. The wave functions and the charge density were expanded with kinetic cutoffs of 40 and 400 Ry, respectively. The first Brillouin zone was sampled at the gamma-point, and the electronic levels were broadened with a marzari-vanderbilt smearing of about 0.02 Ry. The cluster was located in a 30 × 30 × 30 Bohr cubic supercell. The total energy is converged to within 10^{-6} Ry.

We calculated the adsorption energies according to the equation:

$$E_{ads} = E_{total} - E_{cluster} - E_{adsorbate} \quad (1)$$

where E_{total}, $E_{cluster}$ and $E_{adsorbate}$ correspond to the energies of adsorbed species on the Co nanoclusters, the bare Co nanoclusters, and the adsorbates, respectively. So the adsorption energies should be negative for stable adsorption modes. The more negative the adsorption energy is, the stronger the adsorption is. The van der Waals (vdW) corrections are found to make a minor difference, which are not included [48, 49].

Charge density difference of the CO_2 on these Co nanoclusters was calculated based on the equation:

$$\Delta\rho = \rho_{\boldsymbol{CO_2}+cluster} - \rho_{cluster} - \rho_{\boldsymbol{CO_2}} \quad (2)$$

where $\rho_{CO_2+cluster}$, $\rho_{cluster}$ and ρ_{CO_2} correspond to the charge density of the CO_2 adsorbed on these nanoclusters, the bare Co nanoclusters, and the free CO_2, respectively.

The transition states of the dissociation of CO_2 on these Co nanoclusters were

located by the climbing image nudge elastic band (CI-NEB) method [50], and the profiles of potential-energy surfaces (PES) were constructed accordingly. The number of images was set as seven, and the first and the last images were fixed according to the results of adsorption.

3 Results and Discussion

3.1 Structures of Co nanoclusters

The lowest energy structures for Co_n (n = 2 to 58) nanoclusters were predicted from Gupta potential and re-optimized by DFT relaxation. The resulting structures by GA and DFT calculations were then analyzed by comparing the average binding energy per atom, $E_{binding}$, for an n-atom cluster, which is defined as

$$E_{binding} = (E_n - nE_1)/n, \quad (3)$$

where E_n is the energy of Co_n (n = 2 to 58) nanoclusters, and E_1 is the energy of one free Co atom. Fig. 1a shows the average binding energies per atom $E_{binding}$ of Co_n (n = 2 to 58) nanoclusters by both GA and DFT calculations. It is found that $E_{binding}$ increases with the number of atoms as expected for these Co nanoclusters. The same tendency showed in the $E_{binding}$ results using two different methods of GA and DFT proves the validity of our calculations. The binding energy curves can be roughly divided into three regions by both methods: $n \leq 6$ where the binding energy increases rapidly as the cluster size increases, $6 < n < 22$ where the binding energy increases moderately, and $n \geq 22$ where the binding energy increases slowly. On the other hand, it is worth noting that the average binding energy versus n shows mild discontinuities at n = 13 and 55 in the GA curve. Notably, icosahedral shells are filled completely at n = 13, 55… and so forth, indicating that 13-atom and 55-atom nanoclusters possess highly symmetrical icosahedral configurations.

The relative stability of nanoclusters can be picked out by the fragmentation energy and the second difference in energy [51]. The fragmentation energy, $\Delta E_{n,m}$, needed to dissociate a neutral n-atom nanocluster into m-atom and $(n\text{-}m)$-atom

nanoclusters, is given by

$$\Delta E_{n,m} = E_m + E_{n-m} - E_n , \quad (4)$$

where E_m, E_{n-m} and E_n are the total energies of the nanoclusters with *m*, *n-m* and *n* atoms, respectively. It is found that for the fragmentation of the neutral clusters, the most dominant channel is the evaporation of one atom from the cluster. The fragmentation energies for the energetically most favorable channels obtained from Eq. 4 are displayed in Fig. 1b (below, ΔE_n). Clusters with a large fragmentation energies should be more stable. As we can see from Fig. 1b, the relatively stable isomers are found to be *n* = 13, 38, 52, 54 and 55.

The second difference in energy can also classify the relative stability of the clusters. It is defined as

$$\Delta^2 E_n = -2 \times E_n + E_{n+1} + E_{n-1}, \quad (5)$$

where *n* is the number of Co atom. Maxima in $\Delta^2 E_n$ indicate the relative stable structrues. Both the energy differnces, ΔE_n and $\Delta^2 E_n$, were calculated at empirical (Gupta) level. In Fig. 1b (above, $\Delta^2 E_n$), maxima at *n* = 13, 38 and 55 show the relative stablility, showing general agreement with the fragmentation analysis mentioned above. It is noted that the Co nanocluster with the size of *n* = 49 is not taken into consideration in our further DFT calculations for its low symmetry. In addition, the Co nanoclusters with the size of *n* = 52 and 54 only show the marginal stability, which would not be considered in our further DFT calculations.

The magnetization properties of these Co nanoclusters were also studied by DFT calculations, as shown in Fig. 1c. The total magnetization per atom of Co nanoclusters converge to the instrinsic magnetization of the bulk Co, 1.7 μ_B/atom [52], as the number of atoms increases. More specifically, the total magnetization per atom decreases sharply as the size of the nanoclusters increases when $n \leq 6$, it shakes between 1.7 and 1.9 μ_B/atom when $7 < n < 16$, and it becomes realatively stable around 1.75 μ_B/atom when $n \geq 16$.

3.2 Adsorption of CO_2, CO and O on size-selected Co nanoclusters

In this part, we discuss the adsorption of CO_2, CO and O on size-selected Co_{13}, Co_{38} and Co_{55} nanoclusters. The configurations of Co_{13}, Co_{38} and Co_{55} nanoclusters are depicted in Fig. 1b, and high symmetry adsorption sites of these nanoclusters are depicted in Fig. 2. As we can see, both Co_{13} and Co_{55} nanoclusters exhibit icosahedral (Ico) structures, while the Co_{38} nanocluster has a tetrakaidecahedral [28] structure with eight equivalent hexagonal fcc (111)-like faces and six equivalent square fcc (100)-like faces. Different adsorption sites on Co nanoclusters were considered and characterized as top (T1 and T2), bridge (B1, B2 and B3) and hollow (H1, H2 and H3) in this work, as labeled in Fig. 2. All the adsorption sites are universal for CO_2, CO and O. At a top site, the adsorbate adsorbs on the top of Co atom of nanoclusters. At a bridge site, the adsorbate adsorbs over the center of Co-Co bond between the two nearest Co atom. At a hollow site, the adsorbate adsorbs above the center of the square or triangle facet of the Co nanoclusters.

As O is a single atom, the adsorption arrangement of the O atom is simple. For CO adsorption, the molecule prefers the "end-on" configuration [28] with a C atom binding to the metal atom. However, it becomes complicated when considering CO_2 adsorption arrangements. In this work, five CO_2 adsorption modes on Co nanoclusters were investigated and the initial images of these adsorption modes were shown in Fig. 3. These modes are classified by the interaction between Co nanoclusters and the adsorbate, and the capital letters in the notations represent the atoms which bond with Co nanoclusters. Concretely, the modes are named as *-Oco* for the interaction of Co atom with one O atom, *-oCo* for the interaction of Co atom with C atom, *-OCo-* or *-oCO* for the interaction of Co atom with both C and O atoms, and *-OcO-* for the interaction of Co atom with two O atoms. For detailed schematic representation for CO_2 adsorption modes, please see Fig. S1.

The overall adsorption energies of CO_2, CO and O adsorbed on Co_{13}, Co_{38} and Co_{55} nanoclusters are listed in Table S1-3. In general, the more negative the

adsorption energy is, the stronger the adsorption is. The adsorption energies of adsorbed CO_2, CO and O species on Co_{13}, Co_{38} and Co_{55} nanoclusters at the most favorite adsorption sites are summarized in Table 1. All of the configurations of CO_2 adsorbed on Co_{13}, Co_{38} and Co_{55} nanoclusters are displayed in Figs. S2-4. The most favorable adsorption sites for CO_2 on Co_{13}, Co_{38} and Co_{55} nanoclusters are H1, B2, and B1 adsorption sites, respectively. Moreover, the three most favorable adsorption modes are the *-oCo* mode. At each adsorption site, *-oCo* mode with a more negative adsorption energy, corresponds to a stronger adsorption strength. The adsorption energies of CO_2 on Co_{13}, Co_{38} and Co_{55} nanoclusters at the most favorable adsorption site are -1.57, -1.62 and -0.65 eV, respectively, which are more negative than the adsorption energy of CO_2 on Co(100) (-0.42 eV) and Co(110) (-0.61 eV) surfaces at the most favorable adsorption sites [15]. And to complete the comparison, we calculated the adsorption energy of CO_2 on Co(111) surface, displayed in Table S4. That means Co nanoclusters are more beneficial to CO_2 adsorption compared with the Co metal surfaces. And it is found that the most favorable adsorption sites for CO on Co_{13}, Co_{38} and Co_{55} nanoclusters are H1, B2, and H1 adsorption sites, respectively. The most favorable adsorption sites for O atom on Co_{13}, Co_{38} and Co_{55} nanoclusters are H1, B2 and H1 adsorption sites, respectively.

Fig. 4 shows the adsorption energies of CO_2, CO and O at the most favorable adsorption sites, changing with the size of Co nanocluster. It can be found that the adsorption strength of CO_2 and CO on these nanoclusters follows the same order of $Co_{13} \approx Co_{38} > Co_{55}$, while the adsorption strength of O on these nanoclusters follows the order of $Co_{13} > Co_{38} > Co_{55}$. Roughly, for the adsorption of CO_2, CO and O on size-selected Co_{13}, Co_{38} and Co_{55} nanoclusters, the lowest adsorption strength is found for all the different adsorbates on Co_{55} nanocluster. For the different adsorbate on the same size of nanoculster, the adsorption strength follows the order of O > CO > CO_2.

In order to gain a deeper insight of the electronic mechanisms that play a role in

the adsorption properties of CO_2 on these Co nanoclusters with different sizes, analysis was carried out on the partial density of states (PDOS) projected on the Co atoms where CO_2 were adsorbed, as well as on the adatoms (C or O) of CO_2 on these Co nanoclusters. The PDOS and the corresponding charge density difference plots of CO_2 molecule upon Co_{13}, Co_{38} and Co_{55} nanoclusters are shown on the left part in Fig. 5. As shown in PDOS projected on the Co-d of the Co atom where CO_2 adsorbed for Co_{13}, Co_{38} and Co_{55} nanoclusters, there are similar sharp single peaks in PDOS curves of both Co_{13} and Co_{38} nanoclusters at about -1.7 and -1.55 eV, respectively, while there are two distinct peaks for Co_{55} nanocluster at the corresponding positions (-1.26 and -1.65 eV). In addition, there are three strong interaction peaks corresponding to the interaction between C and O atoms, which are the characteristic peaks of CO_2 molecule. Comparing the overlaps between PDOSs of C atoms and Co atoms, more overlaps between PDOSs of O atoms and Co atoms could be observed, meaning greater contribution of O atoms to the electronic states of Co nanocluster. To fully discern the charge transfer differences incurred by nanocluster size, the Löwdin charge values have been displayed on the right part in Fig. 5. It can be found that the whole CO_2 adsorbed on the Co_{13} nanocluster gets more charges (0.79 e) than those on Co_{38} and Co_{55} nanoclusters (both 0.68 e), meaning that CO_2 adsorbed on Co_{13} nanocluster more strongly than on Co_{38} and Co_{55} nanoclusters. Although the integral transferred charges from CO_2 molecule to the Co_{38} and Co_{55} nanoclusters are numerically equal, inequality in charge distribution inside CO_2 molecule could be observed in Fig. 5. As shown, the transferred charges on the nearby atoms in Co_{55} nanocluster are -0.31 and -0.09 e. Part of the transferred charge is used to balance the charge distribution inside the Co_{55} nanocluster. However, for the Co_{38} nanocluster, the values are -0.22 and -0.22 e which means charge distributes equally. This even charge-distribution may be the intrinsic factor leading to stronger adsorption energy of Co_{38} nanocluster toward CO_2 molecule.

In order to get insights into the electronic states of the Co nanoclusters with the adsorption of CO_2, the electronic state of CO_2 adsorbed on Co_{38} nanocluster is plotted in Fig. 6a, corresponding to the single peak at -1.55 eV of the PDOS plot in Fig. 5b. The electronic states of CO_2 adsorbed on Co_{55} nanocluster shown in Fig. 6b and 6c corresponds to the two peaks at -1.65 eV and -1.26 eV, respectively. As shown in Fig. 6a, the electronic clouds could be found equally distributed all over the Co nanocluster. However, for the Co_{55} nanocluster, one electronic state hold the electronic clouds mainly distributing around the Co atoms near CO_2 molecule (labeled in red in Fig. 6b) and the other hold the electron clouds around the symmetric surface Co atoms (labeled in red in Fig. 6c). As a result, there is only one high peak in the PDOSs of Co_{38} nanocluster with the adsorption of CO_2, instead there are two relatively weak peaks in the PDOSs of Co_{55} nanocluster with the adsorption of CO_2. Therefore, the adsorption strength of CO_2 adsorbed on Co_{38} and Co_{55} was different although they transferred same amount charges.

3.3 Dissociation of CO_2 on size-selected Co nanoclusters

In the CI-NEB calculations, the first and the last images for the dissociation reaction should be verified beforehand. The most favorable adsorption configuration of CO_2 can be chosen as the first image, and we would like to predict the most stable coadsorption configuration of CO and O as the last image. To choose the coadsorption site of CO and O, the following rules were obeyed. Firstly, CO molecule and O atom prefer the most favorable adsorption site, and then the inferior favorable adsorption site. Secondly, we give priority to O atom adsorption because O atom can generally adsorb much more strongly compared with CO molecule. Thirdly, it is better for CO molecule and O atom to stay at the same facet. Lastly, CO molecule and O atom should remain an appropriate distance, neither too far nor too close. Following these rules, DFT calculations were used to optimize the several predicted structures and find the most stable configurations of CO and O coadsorption. Eventually, the chosen structures are shown in Fig. 7 as the final

states.

The profiles of potential-energy surfaces (PES) for the dissociation of CO_2 on size-selected Co_{13}, Co_{38} and Co_{55} nanoclusters are displayed in Fig. 7. The summarized energy of free nanocluster and CO_2 was defined as the zero point. For the dissociation of CO_2 on Co_{13} nanocluster, the dissociation barrier of 0.69 eV with an exothermicity of -1.35 eV is found. The transition state (TS) is obtained in which the C-O bond is breaking. Moreover, the dissociation barrier of 0.46 eV with an exothermicity of -0.41 eV is found for the dissociation of CO_2 on Co_{38} nanocluster, where breaking one of the Co-O bonds is found for the TS. Finally, the dissociation barrier of 0.38 eV with an exothermicity of -0.83 eV is found for the dissociation of CO_2 on Co_{55} nanocluster. The TS is obtained in which the C-O bond is breaking meanwhile the Co-C and Co-O bonds are forming. For the dissociation of CO_2 on these size-selected Co nanoclusters, the largest Co_{55} nanocluster possesses the greatest catalytic activity for the dissociation of CO_2, with the smallest reaction barrier of 0.38 eV. However, Co_{55} nanocluster is still small enough for showing special catalytic properties distinct from Co bulk surfaces.

Meanwhile, for the initial states of the Co_{13} nanocluster, the O1-C-O2 angle becomes 123.07° which means a large distortion from 180° corresponding to the linear gas-phase CO_2 molecule. And both C-O bonds length stretched to 1.31 Å compared to 1.17 Å for the free CO_2 molecule. For the Co_{38} cluster, the angle of O1-C-O2 becomes 137.21° and both C-O bonds stretched to 1.25 Å. For the Co_{55} cluster, the angle of O1-C-O2 is 136.92° and two C-O bonds stretched to 1.24 and 1.26 Å, respectively. These results imply that Co_{13} nanocluster upon the adsorption of CO_2 may cause the formation of the most distorted structure among these selected nanoclusters. However, it is not benefit to decrease reaction barrier if the distortion is too strong, since CO_2 molecule needs more energy to change the distorted structure to achieve the appropriate transition states.

4 Conclusions

In summary, Co_{13}, Co_{38} and Co_{55} nanoclusters with relative stable and high symmetry configurations were selected as the most stable high-symmetry structures from Co_n (n = 2 to 58) nanoclusters according to the Gupta potential based on genetic algorithm method. Then, using spin-polarized density functional theory calculations, the adsorption and dissociation properties of CO_2 on size-selected nanoclusters were investigated. It is found that Co_{55} nanocluster possesses the lowest adsorption strength for all the different adsorbates on size-selected Co_{13}, Co_{38} and Co_{55} nanoclusters. For the different adsorbate on the same size of nanoculster, the adsorption strength follows the order of O > CO > CO_2. We subsequently studied the energy barriers for CO_2 dissociation on size-selected Co_{13}, Co_{38} and Co_{55} nanoclusters. Among these size-selected Co_{13}, Co_{38} and Co_{55} naonoclusters, the largest Co_{55} nanocluster was found to possess the greatest catalytic activity to dissociate CO_2, with the smallest reaction barrier of 0.38 eV. It is expected our results can provide a new roadmap for the design and development of new Co catalysts for the dissociation of CO_2.

Acknowledgements

This work is supported by the National Natural Science Foundation of China (21576008, 91334203), BUCT Fund for Disciplines Construction and Development (Project No. XK1501), Fundamental Research Funds for the Central Universities (Project No. buctrc201530 and PT1613-01), and “Chemical Grid Project” of BUCT.

Appendix A. Supplementary data

Supplementary data associated with this article can be found, in the online version, at

References

[1] S.Y. Wu, C.H. Su, J.G. Chang, H.T. Chen, C.H. Hou, H.L. Chen, Adsorption and dissociation of N_2O molecule on Fe(111) surface: A DFT study, Comput. Mater. Sci., 50 (2011) 3311-3314.

[2] A. Aijaz, N. Fujiwara, Q. Xu, From Metal–Organic Framework to Nitrogen-Decorated Nanoporous Carbons: High CO_2 Uptake and Efficient Catalytic Oxygen Reduction, J. Am. Chem. Soc., 136 (2014) 6790-6793.

[3] Z.H. Xiang, S.H. Leng, D.P. Cao, Functional Group Modification of Metal–Organic Frameworks for CO_2 Capture, J. Phys. Chem. C, 116 (2012) 10573-10579.

[4] Z.H. Xiang, X. Peng, X. Cheng, X.J. Li, D.P. Cao, CNT@$Cu_3(BTC)_2$ and Metal–Organic Frameworks for Separation of CO_2/CH_4 Mixture, J. Phys. Chem. C, 115 (2011) 19864-19871.

[5] J.R. Li, J. Yu, W. Lu, L.B. Sun, J. Sculley, P.B. Balbuena, H.C. Zhou, Porous Materials with Pre-Designed Single-Molecule Traps for CO_2 Selective Adsorption, Nat. Commun., 4 (2013) 1538.

[6] H. Tang, D. Lu, C. Wu, Intramolecular Hydrogen Bonds Enhance Disparity in Reactivity between Isomers of Photoswitchable Sorbents and CO2 : A Computational Study, ChemPhysChem, 16 (2015) 1926-1932.

[7] Q. Zhao, Q. Wang, C. Zhang, Z. Du, M. Tian, J. Mi, Effect of chain topology of polyethylenimine on physisorption and chemisorption of carbon dioxide, ChemPhysChem, 16 (2015) 1480-1490.

[8] C.H. Huang, C.S. Tan, A Review: CO_2 Utilization, Aerosol Air Qual. Res., 14 (2014) 480-499.

[9] D. Cheng, F.R. Negreiros, E. Apra, A. Fortunelli, Computational approaches to the chemical conversion of carbon dioxide, ChemSusChem, 6 (2013) 944-965.

[10] K.S. Lackner, A Guide to CO_2 Sequestration, Science, 300 (2003) 1677-1678.

[11] C. Song, Global challenges and strategies for control, conversion and utilization of CO2 for sustainable development involving energy, catalysis, adsorption and chemical processing, Catal. Today, 115 (2006) 2-32.

[12] K. Rajeshwar, N.R. de Tacconi, G. Ghadimkhani, W. Chanmanee, C. Janaky, Tailoring copper oxide semiconductor nanorod arrays for photoelectrochemical reduction of carbon dioxide to methanol, ChemPhysChem, 14 (2013) 2251-2259.

[13] H.J. Freund, H. Behner, B. Bartos, G. Wedler, H. Kuhlenbeck, M. Neumann, CO_2 adsorption and reaction on Fe(111): An angle resolved photoemission (ARUPS) study, Surf. Sci., 180 (1987) 550-564.

[14] C. Liu, T.R. Cundari, A.K. Wilson, CO_2 Reduction on Transition Metal (Fe, Co, Ni, and Cu) Surfaces: In Comparison with Homogeneous Catalysis, J. Phys. Chem. C, 116 (2012) 5681-5688.

[15] V.A. de la Peña O'Shea, S. González, F. Illas, J.L.G. Fierro, Evidence for spontaneous CO_2 activation on cobalt surfaces, Chem. Phys. Lett., 454 (2008) 262-268.

[16] Y.Q. Zhang, G. Jacobs, D.E. Sparks, M.E. Dry, B.H. Davis, CO and CO_2 hydrogenation study on supported cobalt Fischer-Tropsch synthesis catalysts, Catal. Today, 71 (2002) 411-418.
[17] S.G. Wang, D.B. Cao, Y.W. Li, J. Wang, H. Jiao, CO_2 reforming of CH_4 on Ni(111): a density functional theory calculation, J. Phys. Chem. B, 110 (2006) 9976-9983.
[18] G.C. Wang, J. Nakamura, Structure Sensitivity for Forward and Reverse Water-Gas Shift Reactions on Copper Surfaces: A DFT Study, J. Phys. Chem. Lett., 1 (2010) 3053-3057.
[19] C.C. Chang, J.J. Ho, Dissociation of CO_2 on rhodium nanoclusters (Rh_{13}) in various structures supported on unzipped graphene oxide--a DFT study, Phys. Chem. Chem. Phys., 17 (2015) 11028-11035.
[20] H.J. Li, C.H. Yeh, J.J. Ho, The catalytic adsorption and dissociation of carbon dioxide on a double icosahedral Ru_{19} nanocluster – A theoretical study, Chem. Phys. Lett., 585 (2013) 149-152.
[21] A.B. Vidal, L. Feria, J. Evans, Y. Takahashi, P. Liu, K. Nakamura, F. Illas, J.A. Rodriguez, CO Activation and Methanol Synthesis on Novel Au/TiC and Cu/TiC Catalysts, J. Phys. Chem. Lett., 3 (2012) 2275-2280.
[22] V. Iablokov, S.K. Beaumont, S. Alayoglu, V.V. Pushkarev, C. Specht, J. Gao, A.P. Alivisatos, N. Kruse, G.A. Somorjai, Size-Controlled Model Co Nanoparticle Catalysts for CO_2 Hydrogenation: Synthesis, Characterization, and Catalytic Reactions, Nano Lett., 12 (2012) 3091-3096.
[23] M. Zhang, M. El-Roz, H. Frei, J.L. Mendoza-Cortes, M. Head-Gordon, D.C. Lacy, J.C. Peters, Visible Light Sensitized CO_2 Activation by the Tetraaza $[Co_{II}N_4H(MeCN)]^{2+}$ Complex Investigated by FT-IR Spectroscopy and DFT Calculations, J. Phys. Chem. C, 119 (2015) 4645-4654.
[24] S.L. Chan, T.L. Lam, C. Yang, S.C. Yan, N.M. Cheng, A robust and efficient cobalt molecular catalyst for CO_2 reduction, Chem. Commun. (Camb), 51 (2015) 7799-7801.
[25] A.J. Cohen, P. Mori-Sanchez, W. Yang, Challenges for Density Functional Theory, Chem. Rev., 112 (2012) 289-320.
[26] C.J. Cramer, D.G. Truhlar, Density Functional Theory for Transition Metals and Transition Metal Chemistry, Phys. Chem. Chem. Phys., 11 (2009) 10757-10816.
[27] A. Tuxen, S. Carenco, M. Chintapalli, C.-H. Chuang, C. Escudero, E. Pach, P. Jiang, F. Borondics, B. Beberwyck, A.P. Alivisatos, G. Thornton, W.-F. Pong, J. Guo, R. Perez, F. Besenbacher, M. Salmeron, Size-Dependent Dissociation of Carbon Monoxide on Cobalt Nanoparticles, J. Am. Chem. Soc., 135 (2013) 2273-2278.
[28] R.J. Lin, H.L. Chen, S.P. Ju, F.Y. Li, H.T. Chen, Quantum-Chemical Calculations on the Mechanism of the Water-Gas Shift Reaction on Nanosized Gold Cluster, J. Phys. Chem. C,, 116 (2012) 336-342.
[29] D.J. Wales, Global Optimization of Clusters, Crystals, and Biomolecules, Science, 285 (1999) 1368-1372.

[30] R.P. Gupta, Lattice relaxation at a metal surface, Phys. Rev. B, 23 (1981) 6265-6270.
[31] F. Cleri, V. Rosato, Tight-binding potentials for transition metals and alloys, Phys. Rev. B, 48 (1993) 22.
[32] S. Darby, T.V. Mortimer-Jones, R.L. Johnston, C. Roberts, Theoretical study of Cu–Au nanoalloy clusters using a genetic algorithm, J. Chem. Phys., 116 (2002) 1536.
[33] M.S. Bailey, N.T. Wilson, C. Roberts, R.L. Johnston, Structures, stabilities and ordering in Ni-Al nanoalloy clusters, Eur. Phys. J. D, 25 (2003) 41-55.
[34] R.A. Lordeiro, F.F. Guimaraes, J.C. Belchior, R.L. Johnston, Determination of main structural compositions of nanoalloy clusters of Cu_xAu_y (x +y <= 30) using a genetic algorithm approach, Int. J. Quantum Chem., 95 (2003) 112-125.
[35] C. Massen, T.V. Mortimer-Jones, R.L. Johnston, Geometries and segregation properties of platinum-palladium nanoalloy clusters, J. Chem. Soc. Dalton Trans., (2002) 4375-4388.
[36] R.L. Johnston, Evolving better nanoparticles: Genetic algorithms for optimising cluster geometries, Dalton Trans., (2003) 4193-4207.
[37] J.B. Davis, A. Shayeghi, S.L. Horswell, R.L. Johnston, The Birmingham parallel genetic algorithm and its application to the direct DFT global optimisation of Ir_N (N = 10-20) clusters, Nanoscale, 7 (2015) 14032-14038.
[38] S. Núñez, R.L. Johnston, Structures and Chemical Ordering of Small Cu−Ag Clusters, J. Phys. Chem. C, 114 (2010) 13255-13266.
[39] R. Ferrando, A. Fortunelli, R.L. Johnston, Searching for the optimum structures of alloy nanoclusters, Phys. Chem. Chem. Phys., 10 (2008) 640-649.
[40] K.M. Ho, A.A. Shvartsburg, P.B. C., L.Z. Y., W.C. Z., J. Wacker, J.L. Fye, M.F. Jarrold, Structures of medium-sized silicon clusters, Nature, 392 (1998) 582-585.
[41] D.M. Deaven, K.M. Ho, Molecular Geometry Optimization with a Genetic Algorithm, Phys. Rev. Lett., 75 (1995) 288-291.
[42] D.M. Daven, N. Tit, J.R. Morris, K.M. Ho, Structural optimization of Lennard-Jones clusters by a genetic algorithm, Chem. Phys. Lett., 256 (1996) 195-200.
[43] G. Rossi, R. Ferrando, C. Mottet, Structure and chemical ordering in CoPt nanoalloys, Faraday Discuss., 138 (2008) 193.
[44] Q.L. Lu, L.Z. Zhu, L. Ma, G.H. Wang, Magnetic properties of Co/Cu and Co/Pt bimetallic clusters, Chem. Phys. Lett., 407 (2005) 176-179.
[45] P. Giannozzi, S. Baroni, N. Bonini, M. Calandra, R. Car, C. Cavazzoni, D. Ceresoli, G.L. Chiarotti, M. Cococcioni, I. Dabo, A. Dal Corso, S. de Gironcoli, S. Fabris, G. Fratesi, R. Gebauer, U. Gerstmann, C. Gougoussis, A. Kokalj, M. Lazzeri, L. Martin-Samos, N. Marzari, F. Mauri, R. Mazzarello, S. Paolini, A. Pasquarello, L. Paulatto, C. Sbraccia, S. Scandolo, G. Sclauzero, A.P. Seitsonen, A. Smogunov, P. Umari, R.M. Wentzcovitch, QUANTUM ESPRESSO: a modular and open-source software project for quantum simulations of materials, J. Phys.: Condens. Matter, 21

(2009) 395502.
[46] J.P. Perdew, K. Burke, M. Ernzerhof, Generalized Gradient Approximation Made Simple, Phys. Rev. Lett., 77 (1996) 3865-3868.
[47] D. Vanderbilt, Soft Self-Consitent Pseudopotentials in a Generalized Eigenvalue Formalism, Phys. Rev. B 41 (1990) 7892-7895.
[48] Q.G. Jiang, Z.M. Ao, S. Li, Z. Wen, Density Functional Theory Calculations on the CO Catalytic Oxidation on Al-Embedded Graphene, RSC Adv., 4 (2014) 20290-20296.
[49] Y. Tang, Z. Yang, X. Dai, A theoretical simulation on the catalytic oxidation of CO on Pt/graphene, Phys. Chem. Chem. Phys., 14 (2012) 16566-16572.
[50] G. Henkelman, B.P. Uberuaga, H. Jónsson, A climbing image nudged elastic band method for finding saddle points and minimum energy paths, J. Chem. Phys., 113 (2000) 9901.
[51] F.C. Chuang, C. Wang, K. Ho, Structure of neutral aluminum clusters Al_n (2<=n<=23): Genetic algorithm tight-binding calculations, Phys. Rev. B, 73 (2006).
[52] M. Hakamada, F. Hirashima, K. Kajikawa, M. Mabuchi, Magnetism of fcc/fcc, hcp/hcp twin and fcc/hcp twin-like boundaries in cobalt, Appl. Phys. A 106 (2011) 237-244.
[53] M. Dubecký, H. Su, Magnetism in Thiolated Gold Model Junctions, J. Phys. Chem. C, 116 (2012) 17714-17720.

Figure Captions

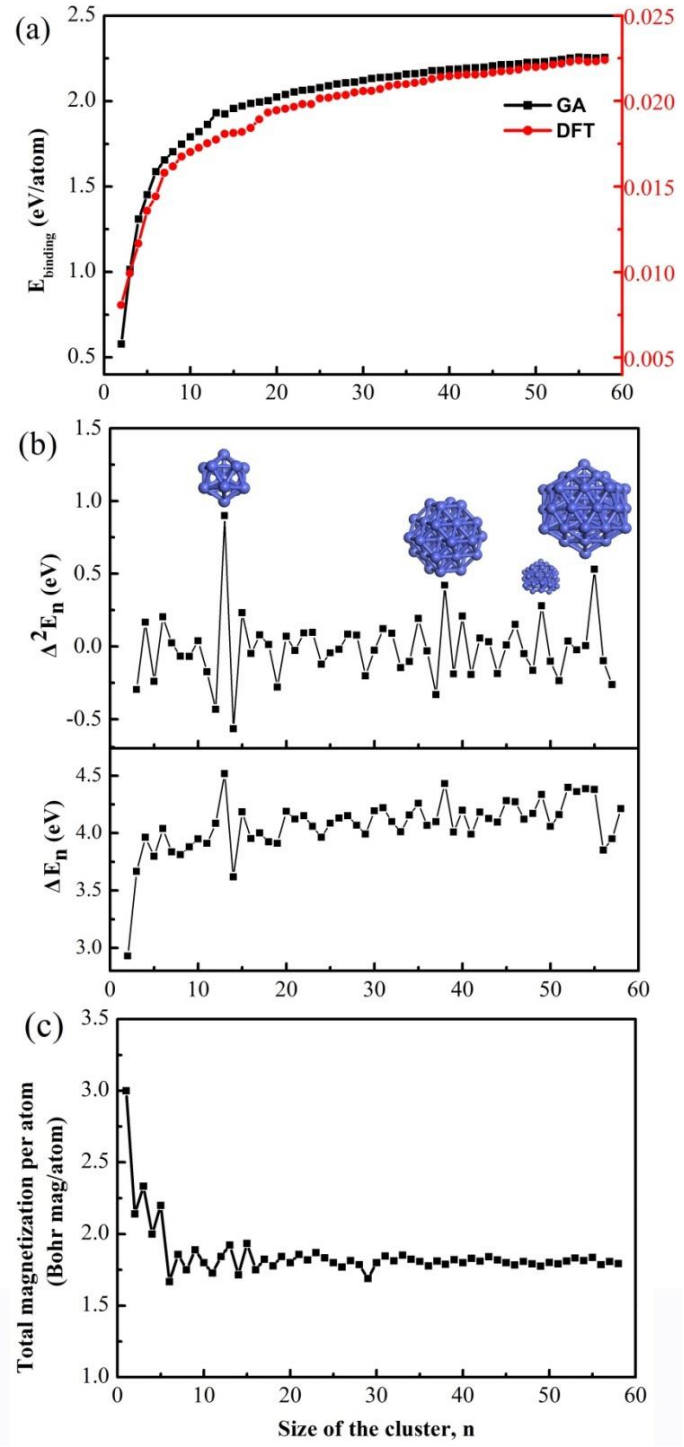

Fig. 1 (a) The binding energy *vs.* size of the cluster. (b) The second difference in energy (above) and the fragmentation energy (below) *vs.* size of the cluster. The most dominant channel of the fragmentation energy is the evaporation of an atom from the cluster, $\Delta E_{n,1} = E_1 + E_{n-1} - E_n$. (c) The total magnetization per atom

(μ_B/atom) *vs.* size of the cluster.

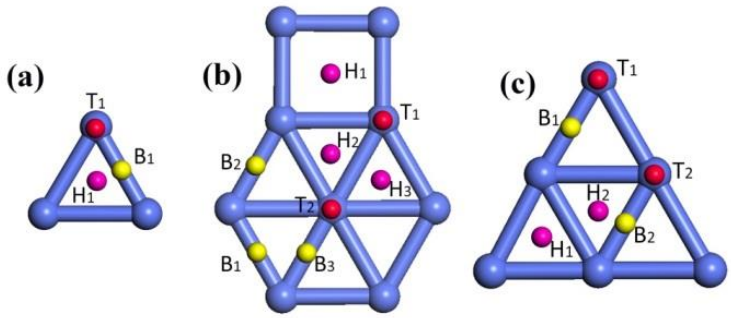

Fig. 2 High symmetry adsorption sites of (a) Co_{13}, (b) Co_{38} and (c) Co_{55} nanoparticles. T1 and T2 represent the top sites; B1, B2 and B3 represent the bridge sites; H1, H2 and H3 represent the hollow sites.

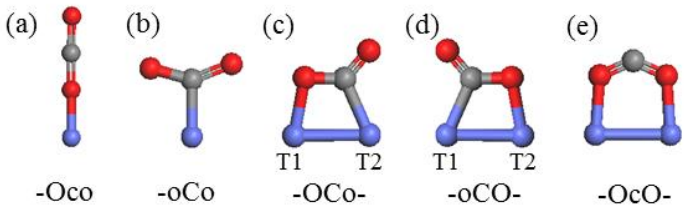

Fig. 3 Schematic representation of initial adsorption modes of CO_2 on the Co_n nanoclusters: (a) *–Oco*, (b) *–oCo*, (c) *–OCo-*, (d) *–oCO-*, (e) *–OcO-*. (Red, O; grey, C; blue, Co.)

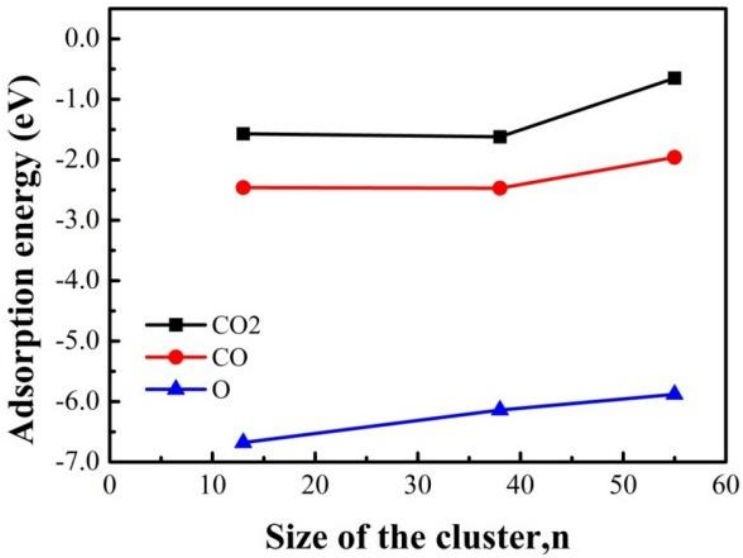

Fig. 4 Adsorption energy of CO_2, CO, O on Co_{13}, Co_{38} and Co_{55} nanoclusters at the most favorable adsorption sites *vs.* size of the cluster.

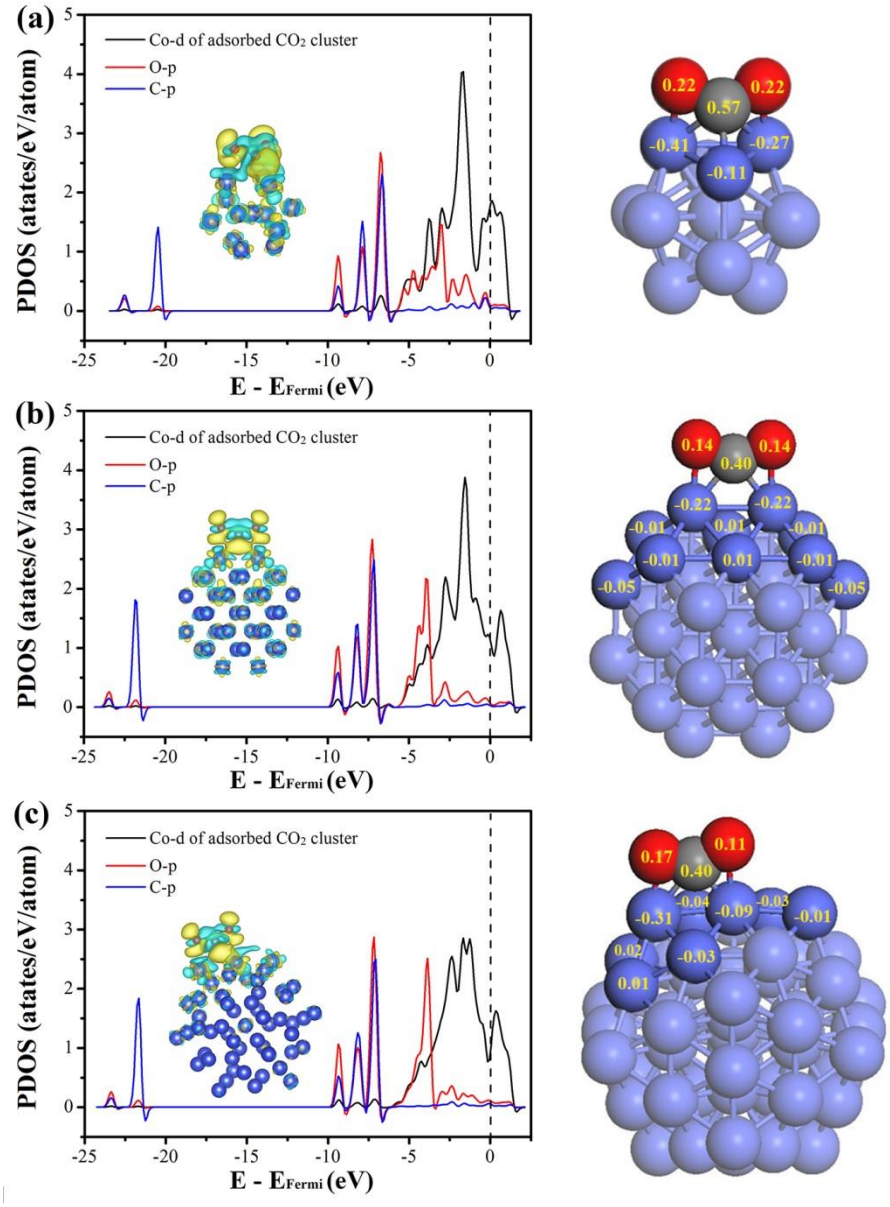

Fig. 5 The partial density of states projected on the Co atom where CO_2 were adsorbed and the adatoms (C or O) of CO_2 molecule upon (a) Co_{13}, (b) Co_{38} and (c) Co_{55} nanoclusters, and (inset) charge density difference ($\Delta\rho = \rho_{CO_2+cluster} - \rho_{CO_2} - \rho_{cluster}$) plot (left part). The light blue and the yellow represent electron accumulation and depletion, respectively. The isosurface charge density was taken to be 0.002 e/Å [53]. And the Löwdin charge (in *e*) analysis of CO_2 and the nearby cobalt atoms on Co clusters (red atom, O; grey atom, C; blue atom, Co) (right part). The positive value indicates positive charge and the minus value indicates negative charge.

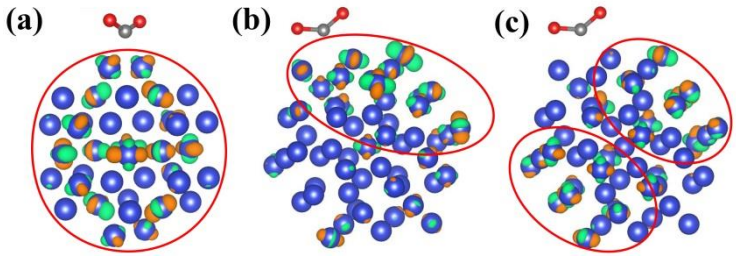

Fig. 6 The electronic states plots of CO_2 absorbed on (a) Co_{38} and (b, c) Co_{55} nanoclusters of the corresponding peaks at -1.5 eV in the PDOS plots. The red circles show the main distribution areas of electron clouds. The isosurface charge density was taken to be 0.005 e/Å.

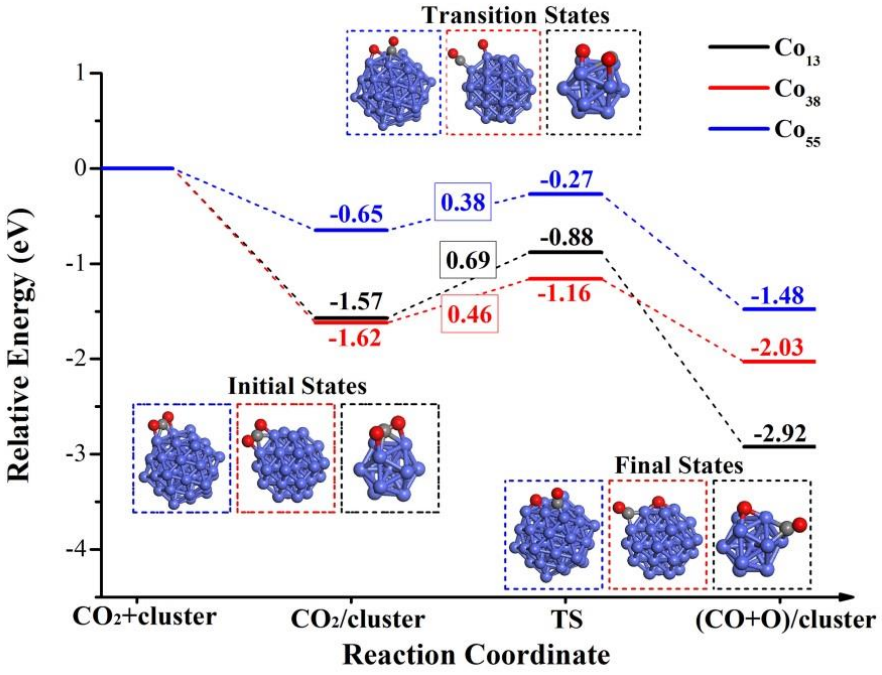

Fig. 7 Calculated reaction coordinates for the dissociation of CO_2 on Co_{13}, Co_{38} and Co_{55} nanoclusters. The energy is relative to the total energy of the free nanocluster and CO_2 molecule.

Table 1 Gupta potential parameters for Co nanoclusters.

	A/eV	ξ/eV	p	q	r_o/ Å
Co-Co	0.1888	1.9066	8.80	2.96	2.507

Table 2 Calculated adsorption energies (in eV), O1-C-O2 angle (in degree) of adsorbed CO_2, CO and O species on Co_{13}, Co_{38} and Co_{55} nanoclusters of the most favorite configurations after relaxation.

nanocluster	adsorbate	site	E_{ads}	∠O1-C-O2
Co_{13}	CO_2	H1, –oCo	-1.57	123.071
	CO	H1	-2.46	-
	O	H1	-6.68	-
Co_{38}	CO_2	B2, –oCo	-1.62	137.214
	CO	B1	-2.47	-
	O	B2	-6.14	
Co_{55}	CO_2	B1, –oCo	-0.65	136.918
	CO	H1	-1.96	-
	O	H1	-5.88	-